Nonequilibrium Ising model on a two-dimensional additive small-world network

R. A. Dumer [*] and M. Godoy [†]
Instituto de Física, Universidade Federal de Mato Grosso, 78060-900 Cuiabá MT, Brazil

(Received 18 October 2022; accepted 28 March 2023; published 21 April 2023)

In this work, we have studied the Ising model with one- and two-spin flip competing dynamics on a two-dimensional *additive* small-world network (A-SWN). The system model consists of an $L \times L$ square lattice where each site of the lattice is occupied by a spin variable that interacts with the nearest-neighbor spins and it has a certain probability p of being additionally connected at random to one of its farther neighbors. The dynamics present in the system can be defined by the probability q of being in contact with a heat bath at a given temperature T and, at the same time, with a probability of $(1-q)$ the system is subjected to an external flux of energy into the system. The contact with the heat bath is simulated by one-spin flip according to the Metropolis prescription, while the input of energy is mimicked by the two-spin flip process, involving a simultaneous flipping of a pair of neighboring spins. We have employed Monte Carlo simulations to obtain the thermodynamic quantities of the system, such as the total m_L^{F} and staggered m_L^{AF} magnetizations per spin, the susceptibility χ_L, and the reduced fourth-order Binder cumulant U_L. We have built the phase diagram for the stationary states of the model in the plane T versus q, showing the existence of two continuous transition lines for each value of p: one line between the ferromagnetic F and paramagnetic P phases and the other line between the P and antiferromagnetic AF phases. Therefore, we have shown that the phase diagram topology changes when p increases. Using the finite-size scaling analysis, we also obtained the critical exponents for the system, where, varying the parameter p, we have observed a different universality class from the Ising model in the regular square lattice to the A-SWN.

DOI: 10.1103/PhysRevE.107.044115

I. INTRODUCTION

In the 1960s, the dynamic behavior of the Ising model was successfully described by the Glauber [1] and Kawasaki [2] mechanisms. This instigated interest in the competition between the Glauber and Kawasaki stochastic process, where Kawasaki proposes the two-spin exchange and Glauber the spin-flip mechanism, both to act in the kinetic Ising model simulating the system relaxing to the lowest energy state. On the other hand, in a competing dynamic scenario, we have a system in contact with a heat bath while exposed to an external energy flux, where the Glauber mechanism is responsible for simulating the system in contact with the heat bath and the Kawasaki mechanism is modified to mimic the system exposed to an external energy flux, once the external energy flux increases the energy of the system. The Kawasaki mechanism only exchanges the state of two connected spins, these spins being chosen at random, thus conserving the magnetization, i.e., the order parameter. Therefore, with that characteristic, the Kawasaki mechanism is only useful in diffusion problems, being necessary an additional flipping mechanism, as Glauber mechanism, to start from a random state and reach an stationary state with different magnetization as used in Monte Carlo simulations. This competition can be simulated by the Glauber process with probability q simulating the system in contact with a heat bath at a temperature T, and at the same time, with probability $(1-q)$, the Kawasaki process mimics an input of energy into the system [3]. Each of these dynamical processes singly satisfies the detailed balance condition, which drives the system toward equilibrium. However, when both can act in the system, the detailed balance is no longer satisfied and it is forced out of equilibrium.

The Ising model on a regular square lattice has a universality class given by a set of critical exponents and a critical temperature, both well known exactly at the equilibrium state [4]. Therefore, the stationary nonequilibrium states were obtained by the two competing dynamic processes described above, and a self-organization is observed by the disappearance of the ordered ferromagnetic F phase in the transition to the paramagnetic P phase, and identification of the ordered antiferromagnetic AF phase, as we increase the flow of energy into the system [5]. However, through the Monte Carlo simulations (MC) the critical exponents of the system have been obtained, and because it is a system with the same symmetry, spatial dimension, and range interactions, the exponents are the same as at the equilibrium state model and known exactly [6].

In the same way, Godoy and Figueredo [7,8] investigated the mixed-spin Ising model with two competing dynamics, where it is not accepted to exchange spin states between sublattices with different spin types. Therefore, it is necessary to change the Kawasaki mechanism from the usual competing dynamics for one that does not exchange the state of spins in the lattice. This change leads to the use of the two-spin flip mechanism that now does not depend on an additional dynamic in the simulation. In these works that use the

[*] rafaeldumer@fisica.ufmt.br
[†] mgodoy@fisica.ufmt.br

two-spin flip mechanism, like with the Kawasaki mechanism, it is used to mimic an input of energy into the system. The input of energy is made by the form of the transition rate of the spin states, because a new state is only if it increases the energy of the system, as would be expected for a system exposed to an external energy flux, would it be accepted. Thus, the competing dynamic was made by the one- and two-spin flip mechanisms, and even with that, they have also obtained the self-organization phenomena [7]. Based on the critical behavior of the system, the universality class of the system is the same as that of the Ising model with only spin-1/2 [8]. Therefore, in the nonequilibrium models, the universality class of the stationary critical behavior is the same as in the equilibrium models. All of these works were studied on regular square lattices.

By using graph theory, Watts and Strogatz quantify the properties of small-world phenomena as demonstrated in Milgram's 1967 study [9]. As an underlying assumption of the Watts-Strogatz model (WS model) [10], vertices of graphs are sites of networks, and edges are connections between sites of the networks. By introducing a disorder parameter p, as the probability of randomly rewiring each one of the connections in a regular lattice, we can obtain the SWN in specific regions in the interval $0 < p \leqslant 1$. The SWN regime is identified in regions of p where the network possesses local clustering, $C(p)$, of a regular lattice but at the same time has an average distance between any two sites, $l(p)$, characteristic of a random lattice. In addition to the WS model, some variants of this model were also developed to describe the properties of a SWN. One of these variants [11] uses a regular square lattice, and we can add a long-range interaction to each site with a certain probability p. This leads to a small typical separation, preserving the clustering property of a regular lattice. While in the WS model the connections of a regular lattice are rewired, also called rewiring SWN (R-SWN) [10], the variant where long-range interactions are added on sites of a regular lattice is known as additive SWN (A-SWN) [11], and both networks always preserve the characteristic of $C(p)$ and $l(p)$ of a SWN.

These networks have been used in numerous physical models since the initial SWN model was put forth [12–16], including the Ising model in one dimension (1D), 2D, and 3D for the investigation of the critical phenomena at equilibrium system [17–24]. According to these findings for the Ising model, an order to the disorder phase transition is established for $T \neq 0$ with $0 < p \leqslant 1$, and it is seen that the addition of long-range interactions changes the critical behavior of the system.

For the interesting behavior of the Ising model at the equilibrium SWN, its investigation was also carried out about the nonequilibrium phase transitions by the competing dynamics: analytically in 1D [25], by MC simulations in 2D [26], and by the Gaussian model in 3D [27]. In all of these works they have been using the competition between the Glauber and Kawasaki dynamics and have no conclusions about the mean-field critical behavior observed at the equilibrium Ising model on a SWN [18,20–22,24,28]. However, the AF-P and F-P phase transitions are in 2D and 3D systems, characteristic of the self-organization phenomena, and they are observed in all of the other systems at the nonequilibrium state by the competing dynamics.

In the present work, we have investigated the Ising model in a two-dimensional A-SWN, where each site of the network is occupied by a spin variable spin-1/2 that can assume values ± 1. We limit by 1 the number of long-range interactions that each site can receive with probability p and divide the network into two sublattices; each new interaction created should connect these sublattices. The system is in a nonequilibrium regime by competing between two dynamic processes that do not conserve the order parameter: With competition probability q, the one-spin flip process simulates the system in contact with a heat bath at temperature T, and with competition probability $1 - q$ the two-spin flip process mimics the system subjected to an external energy flux into it. Therefore, the system is studied at the nonequilibrium regime due to competing dynamics. We verified the phase transition between the AF and F ordered phases to the P disordered phase, and if the system is in this A-SWN regime, then it exhibit the same mean-field critical behavior observed at equilibrium systems with long-range interactions by the A-SWN, see Ref. [28]. The behavior of the phase transitions, phases diagrams, and critical exponents by finite-size scaling theory (FSS) analysis also are described and compared with those of Ref. [28].

This work is organized as follows: In Sec. II, we describe the model, the network, and the motion equations for the nonequilibrium Ising model. In Sec. III, we present the MC simulation method used. The behavior of the phase transitions, phase diagrams, and critical exponents by FSS analysis is described in Sec. IV. Finally, in Sec. V, we present our conclusions.

II. MODEL

The Ising model with $N = L^2$ spins $\sigma_i = \pm 1$ on a regular square lattice $L \times L$, periodic boundary conditions, and a nearest-neighbor ferromagnetic interaction of strength J has been studied in this work [see Fig. 1(a)]. On the other hand, with a certain probability p, we can add one long-range interaction J_{ik} to each site of that regular square lattice. We divided the system into two sublattices to add the long-range interactions J_{ik}, in which one sublattice plays the role of central spins, while the other sublattice contains the spins in which the central spins can connect to beyond their nearest neighbors. Thus, to choose a long-range interaction J_{ik} for a site i, the sublattice of i will be the sublattice of the central spins, and then we choose randomly a site k from another sublattice. If site k is not one of the nearest neighbors already naturally coupled with i, then we picked a random number $0 < r < 1$, and if $r \leqslant p$ (with p predefined), then we couple the site k to the neighbors of site i, and for the site k we couple the site i to its neighbors. The attempt to add a long-range interaction J_{ik} is made once to each site that does not have a long-range interaction J_{ik} in the network, and as result, we have a network with an average coordination number $z = 4 + p$. Therefore, we have the following examples: (i) for $p = 0$, i.e., the probability of adding a long-range interaction J_{ik} to any site on the lattice is zero, and therefore we have a regular square lattice [see Fig. 1(a)] and (ii) for $p = 0.5$, we are in the A-SWN regime because in addition to the conservation of $C(p)$, and we also have an average short path length between network sites, through the shortcuts created by the long-range interaction

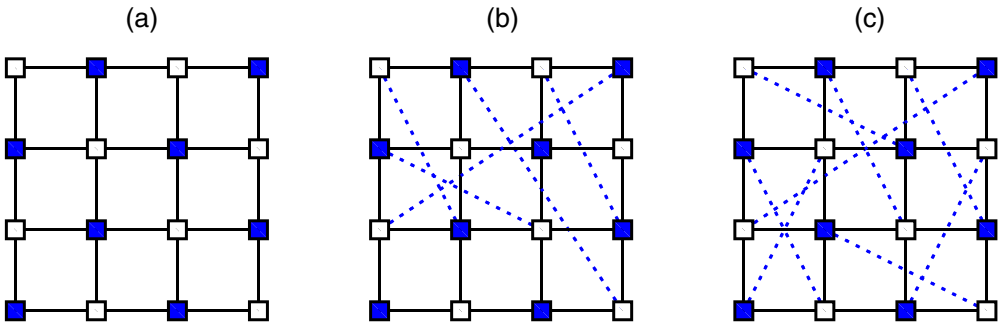

FIG. 1. Schematic representation of the system and the A-SWN. The blue (dark gray) square dots indicate the sites on one of the sublattices, the white square dots are the sites on the other sublattice, the solid black lines are the nearest-neighbor interactions J between pairs of spins, and the blue-dashed lines are long-range interaction J_{ik} added to the network with a certain probability p. (a) For $p = 0$, (b) for $p = 0.5$, and (c) for $p = 1$.

J_{ik} added between the sublattices, see Fig. 1(b); finally, for $p = 1$, all sites on the network have a long-range interaction J_{ik} connecting the two sublattices, and consequently, it is the network with the shortest typical separation between the sites on the network, see Fig. 1(c).

Thus, as the regular structure in $p = 0$ remains unaltered [Fig. 1(a)], we have a high local clustering for any value of p, and conform we increase p, the long-range interaction J_{ik} is added to the network, creating shortcuts between the sites that in the regular lattice, $p = 0$, would be more distant, consequently decreasing the typical distance $l(p)$ of the network. The $l(p)$ scales linearly $l(p \to 0) \sim L/2$ and logarithmically $l(p \to 1) \sim \ln(L^{1.77})$, where these regimes referred to the "large-world" and "small-world," respectively. The crossover between these regimes occurs when the average number of shortcuts is about 1, or in other words, we can say in the SWN regime when $p \gtrsim 2L^{-2}$ [5]. So, our study is based on $p \geqslant 0.25$ values, where the A-SWN is found and the decay of l as a function of p is less pronounced, i.e., having roughly the same value of l.

The ferromagnetic Ising spin energy is described by the Hamiltonian of the form:

$$\mathcal{H} = -J \sum_{\langle i,j \rangle} \sigma_i \sigma_j - \sum_{\langle i,k \rangle} J_{ik} \sigma_i \sigma_k, \tag{1}$$

where J is the nearest-neighbor ferromagnetic interaction and J_{ik} is the long-range interaction on the A-SWN. The first sum is over all the pairs of nearest-neighbor spins on the regular square lattice and the second sum is made over all the pairs of spins (i, k) connected through long-range interaction on the A-SWN. Here we always are considering $J_{ik} = J = 1$.

We are dealing with the nonequilibrium Ising model and in a SWN, being the time evolution of the states of the system governed by two competing dynamical processes: one simulating the contact of the system with a heat bath at temperature T, with the one-spin flip process and probability q to occur, and at the same time but with probability $(1 - q)$ to occur, the system is subjected to an external flux of energy into the system with the two-spin flip process, where in addition to flipping the chosen spin, it simultaneously flips one of its randomly chosen neighbors.

Let us call $p(\{\sigma\}, t)$ the probability of finding the system in the state $\{\sigma\} = \{\sigma_1, \ldots, \sigma_i, \ldots, \sigma_j, \ldots \sigma_N\}$ at time t, the motion equation for the probability states evolve in time according to the master equation

$$\frac{d}{dt} p(\{\sigma\}, t) = qG + (1 - q)V, \tag{2}$$

where qG represents the process of relaxation of the spins in contact with a heat bath at temperature T, favoring the lowest energy in the system, and $(1 - q)V$ represents the process independent of the temperature, where the energy of the system increases by one external flow of energy into it. G and V are described by

$$G = \sum_{i,\{\sigma'\}} [W(\sigma_i \to \sigma_i') p(\{\sigma\}, t) - W(\sigma_i' \to \sigma_i) p(\{\sigma'\}, t)], \tag{3}$$

$$V = \sum_{i,j,\{\sigma'\}} [W(\sigma_i \sigma_j \to \sigma_i' \sigma_j') p(\{\sigma\}, t) - W(\sigma_i' \sigma_j' \to \sigma_i \sigma_j) p(\{\sigma'\}, t)], \tag{4}$$

where $\{\sigma'\}$ denotes the spin configurations after the spin flipping, $W(\sigma_i \to \sigma_i')$ is the transition rate between states in the one-spin flip process, and $W(\sigma_i \sigma_j \to \sigma_i' \sigma_j')$ the transition rate between the states in the two-spin flip process, with the order parameter being conserved in none of the dynamic processes.

If $0 < q < 1$, then the two dynamics processes have nonnull probability to be chosen and act in the system, the detailed balance is not satisfied, and it is forced out of equilibrium. As these processes favor the states of higher and lower energy of the system, with the competition it is possible to find stationary states for the order parameter in the AF, F, and P phases. It is worth noting that to reach the stationary state in the AF phase was of fundamental importance to use the J_{ik} between the sublattices because of the antiparallel ordering in which this phase is characterized.

III. MONTE CARLO SIMULATIONS

Let (k, l) and (k', l') be the coordinates of a site in our two-dimensional SWN and one of your neighbors, respectively. The periodic boundary conditions were used in all our simulations. Starting the initial state of the system with all spins aligned in the same direction, a new configuration is

generated by the following the Markov process: For a given temperature T, competition probability q, and additive probability p, we choose a random spin from the lattice, i.e., we choose a coordinate k and l at random. Then we generate a random number ξ between zero and 1, and if $\xi \leqslant q$, then we choose the one-spin flip process. In this process, the flipping probability is dependent on $W(\sigma_{kl} \to \sigma'_{kl})$, which is given by the Metropolis prescription as follows:

$$W(\sigma_{kl} \to \sigma'_{kl}) = \begin{cases} \exp(-\Delta E_{kl}/k_B T) & \text{if} \quad \Delta E_{kl} > 0 \\ 1 & \text{if} \quad \Delta E_{kl} \leqslant 0 \end{cases}, \tag{5}$$

where ΔE_{kl} is the change in the energy after flipping the spin $\sigma_{kl} \to \sigma'_{kl}$, k_B is the Boltzmann constant, and T is the absolute temperature, and thus the new state is accepted if $\Delta E_{kl} \leqslant 0$, and in the case of $\Delta E_{kl} > 0$ we choose another random number $1 < \xi_1 < 0$ and if $\xi_1 \leqslant \exp(-\Delta E_{kl}/k_B T)$, then the new state is also accepted, but if none of the conditions are satisfied, then we do not change the state of the system. On the other hand, if $\xi > q$, then the two-spin flip process is chosen. In this case, in addition to the spin σ_{kl}, we also randomly choose one of its neighbors $\sigma_{k'l'}$, which can be either the nearest neighbor or the farthest neighbor coming from a J_{ik}. In this process, the two spins chosen are flipping simultaneously, and for that the two-spin flip probability is dependent on $W(\sigma_{kl}\sigma_{k'l'} \to \sigma'_{kl}\sigma'_{k'l'})$, which is given by

$$W(\sigma_{kl}\sigma_{k'l'} \to \sigma'_{kl}\sigma'_{k'l'}) = \begin{cases} 0 & \text{if } \Delta E_{kl,k'l'} \leqslant 0 \\ 1 & \text{if } \Delta E_{kl,k'l'} > 0 \end{cases}, \tag{6}$$

where $\Delta E_{kl,k'l'}$ is the change in the energy after flipping the spins σ_{kl} and $\sigma_{k'l'}$. Thus, in this process, the new state is just accepted if $\Delta E_{kl,k'l'} > 0$.

Repeating the Markov process N times, we have one Monte Carlo Step (MCS). In our simulations, for $p \neq 0$, we have waited for 2×10^4 MCS for the system to reach the stationary state for all the lattice sizes. We used more 5×10^3 MCS to calculate the thermal averages of the quantities of interest. The average over the samples was done using 25 independent samples for any lattice. On the other hand, for the case $p = 0$, we needed to wait for 5×10^5 MCS to reach the equilibrium state, and more 3×10^5 MCS to calculate the thermal average, only over one sample.

The measured thermodynamic quantities in our simulations are the total magnetization per spin m_L^{F}, the staggered magnetization per spin m_L^{AF}, the magnetic susceptibility χ_L, and the reduced fourth-order Binder cumulant U_L:

$$m_L^{\mathrm{F}} = \frac{1}{N}\left[\left\langle \sum_{kl} \sigma_{kl} \right\rangle\right], \tag{7}$$

$$m_L^{\mathrm{AF}} = \frac{1}{N}\left[\left\langle \sum_{kl} (-1)^{(k+l)} \sigma_{kl} \right\rangle\right], \tag{8}$$

$$\chi_L = \frac{N}{k_B T}[\langle m^2 \rangle - \langle m \rangle^2], \tag{9}$$

$$U_L = 1 - \frac{[\langle m^4 \rangle]}{3[\langle m^2 \rangle^2]}, \tag{10}$$

where $[\ldots]$ denotes the average over the samples, $\langle \ldots \rangle$ is the thermal average over the MCS in the stationary state, and m can be m_L^{F} or m_L^{AF} in Eqs. (9) and (10). The lattice sizes from $L = 24$ to $L = 256$ are simulated and the data are analyzed via FSS. These Eqs. (7), (8), (9), and (10) obey the following FSS relations in the neighborhood of the stationary critical point λ_C:

$$m_L = L^{-\beta/\nu} m_0(L^{1/\nu}\varepsilon), \tag{11}$$

$$\chi_L = L^{\gamma/\nu} \mathcal{X}_0(L^{1/\nu}\varepsilon), \tag{12}$$

$$U_L = U_0(L^{1/\nu}\varepsilon), \tag{13}$$

where $\varepsilon = (\lambda - \lambda_C)/\lambda_C$ and λ can be T or q. Here m_0, χ_0, and U_0 are scaling functions, where β, γ, and ν are the critical exponents related to magnetization, susceptibility, and the length correlation, respectively. The derivative of Eq. (13) with respect to the parameter λ gives us the following scaling relation:

$$U'_L = \frac{L^{1/\nu}}{\lambda_C} U'_0(L^{1/\nu}\varepsilon). \tag{14}$$

We have determined the critical exponent relations β/ν, γ/ν, and ν from the slope of a log-log plot of $m_L(\lambda_C)$, $\mathcal{X}_L(\lambda_C)$, or $U'_L(\lambda_C)$ versus lattice size L, respectively. We also have used another alternative method to estimate the values of the critical exponents and the data collapse from the scaling functions.

IV. RESULTS AND DISCUSSIONS

In this section, we illustrate and discuss the results of the magnetic properties of the Ising model on a 2D A-SWN at the nonequilibrium regime by the two competing dynamics. For the study about the critical behavior and phase transitions at the nonequilibrium system, it was convenient to fix the temperature T and additive probability p and to use the competition parameter q as a variable to transit between the ordered to disordered phases in the regions of T and p of the phase diagram. This is convenient because the two-spin flip mechanism is independent of the temperature T, and in the present work we do not have used p as a variable to identify the phase transitions.

Before studying the thermal phase diagrams, we will present the best results for the behavior of thermodynamic quantities and critical point values. These results were obtained where most sites have the same coordination number $z = 5$. Therefore, in Fig. 2, we have shown one of the best results for the thermodynamic quantities obtained in the stationary state as a function of q for fixed $p = 0.75$ and $T = 1$. We can see the self-organization in the system by finding an AF phase, which is represented in the staggered magnetization m_L^{AF}. This is because for low values of q we have the transition between the AF to P phases [see Fig. 2(a)] and from this P phase to the ordered F phase [see m_L^{F} in Fig. 2(b)] as we decrease the flow of energy into the system ($q \to 0$). For these magnetizations, we also have their respective reduced fourth-order Binder cumulants, U_L^{AF} [Fig. 2(c)] and U_L^{F} [Fig. 2(d)] beyond the magnetic susceptibilities χ_L^{AF} [Figs. 2(e)] and χ_L^{F} [Fig. 2(f)].

The thermodynamic quantities for the other p values in the A-SWN regime, such as $p = 0.25$, $p = 0.5$, $p = 0.75$, and

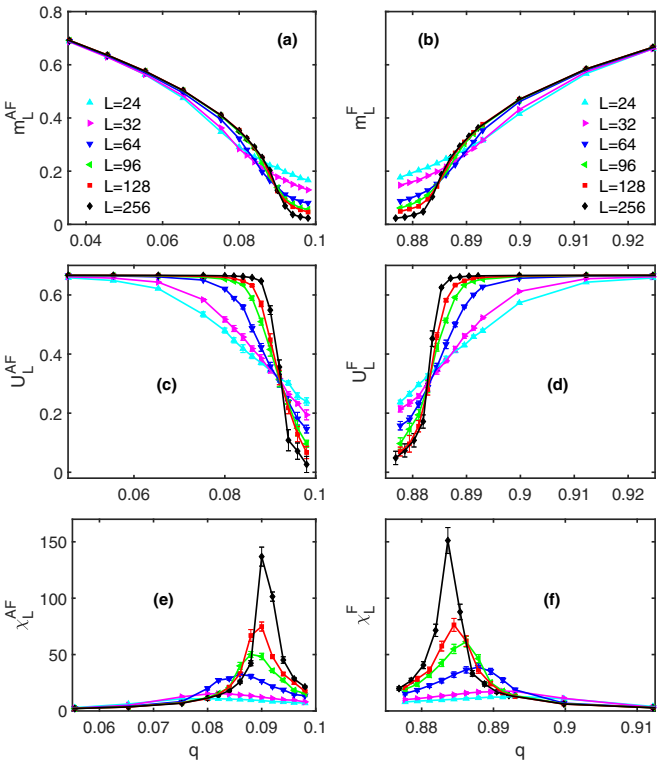

FIG. 2. Thermodynamic quantities in the phase transitions of the nonequilibrium system, with $p = 0.75$, $T = 1$, and lattice sizes L shown in the figures. (a) Staggered magnetization m_L^{AF}, (c) and (e) the Binder cumulant U_L^{AF} and the staggered susceptibility χ_L^{AF}, respectively. (b) Total magnetization m_L^{F} of the system is represented, the Binder cumulant U_L^{F} (d), and the total susceptibility χ_L^{F} (f). The error bars in the magnetization are smaller than the size of the symbols, so for a better interpretation of the results, these were omitted.

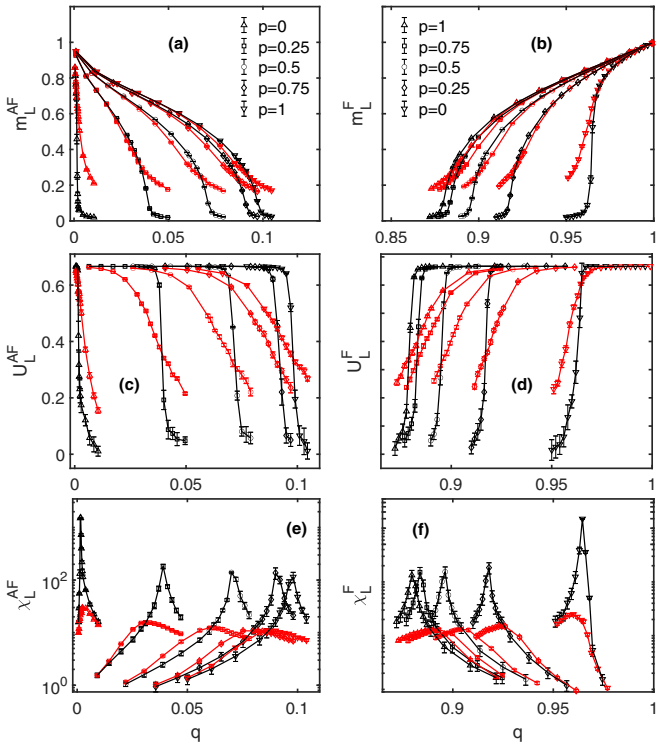

FIG. 3. Thermodynamic quantities as a function of q, for different values of p as indicated in the figures. We fixed the value of $T = 1$, and for lattice sizes $L = 256$ (black curves), and $L = 24$ [red (light gray) curves]. (a) Staggered magnetization m_L^{AF}; (c) and (e) the Binder cumulative U_L^{AF} and staggered susceptibility χ_L^{AF}, respectively. (b) Total magnetization m_L^{F} of the system is represented, the Binder cumulant U_L^{F} (d), and the total susceptibility χ_L^{F} (f).

$p = 1$, have also been computed. In the order to compare the behavior during phase transitions, we also exhibited the same thermodynamic quantities in the conventional square lattice Ising model, $p = 0$, in Fig. 3. These result can see in details for the m_L^{AF} and m_L^{F} in Figs. 3(a) and 3(b), respectively, U_L^{AF} in Fig. 3(c) and U_L^{F} in Fig. 3(d), in addition to χ_L^{AF} in Fig. 3(e) and χ_L^{F} in Fig. 3(f). We have presented only the smaller ($L = 24$) and the larger ($L = 256$) linear lattice size and they are enough so that we can observe the finite-size behavior and the critical point change q_c as we increase p. On the other hand, for the calculation of q_c, we have used all six lattice sizes of the system.

In order to evaluate the q_c, we have employed two methods. First, we obtained by extrapolating the susceptibility discontinuity to when $L \to \infty$, which returns $q_c(\infty)$, using finite lattice sizes $24 \leqslant L \leqslant 256$, in the plot of maximum susceptibility as a function of $1/L$. Second, we obtained by the crossing of the Binder cumulant curves for the different lattice sizes L. In Fig. 4 the values of q are displayed where the susceptibility has its maximum value, $\chi_L^{\max}$, as a function of $1/L$ for the values of p selected. We also have the best fit of the points, which is a linear fit, and for the extrapolation, when $L \to \infty$, we have the estimated of q_c by using the linear coefficient, i.e., we have made the infinite-size extrapolation in according to $q(\chi_L^{\max}) - q_c(\infty) = \alpha L^{-1}$. By extrapolation, the critical points $q_c(\infty)$ in the transition between the AF-P phases are represented in Fig. 4(a) and the transition between the F-P phases are represented in Fig. 4(b).

The critical point values using magnetic susceptibility data, q_c^{χ}, and their respective errors are exhibited in Table I for the transition between the AF-P phases, and in Table II for the transition between F-P phases. In these transitions, we also have used the crossing of the Binder cumulant curves in the selected lattice sizes $24 \leqslant L \leqslant 256$ to obtain the another estimate for the critical points, q_c^U, and the characterization of the second-order phase transition in the system [30–33]. q_c^U are shown in Table III and in Table IV for AF-P and F-P phase transitions respecively. The critical points obtained in both methods are equivalent.

TABLE I. Critical competition probability q_c, based on the extrapolating of the susceptibility discontinuity and in the AF-P phase transition, for $T = 1$.

p	q_c^{χ}	β/ν	γ/ν	ν
0	0.00149 ± 0.0001	0.16 ± 0.05	1.77 ± 0.03	1.04 ± 0.09
0.25	0.03966 ± 0.002	0.46 ± 0.07	1.07 ± 0.06	1.07 ± 0.03
0.5	0.07176 ± 0.003	0.45 ± 0.04	1.06 ± 0.04	0.96 ± 0.09
0.75	0.09062 ± 0.002	0.46 ± 0.03	1.04 ± 0.02	1.02 ± 0.05
1.0	0.09774 ± 0.002	0.48 ± 0.02	1.05 ± 0.02	1.06 ± 0.08

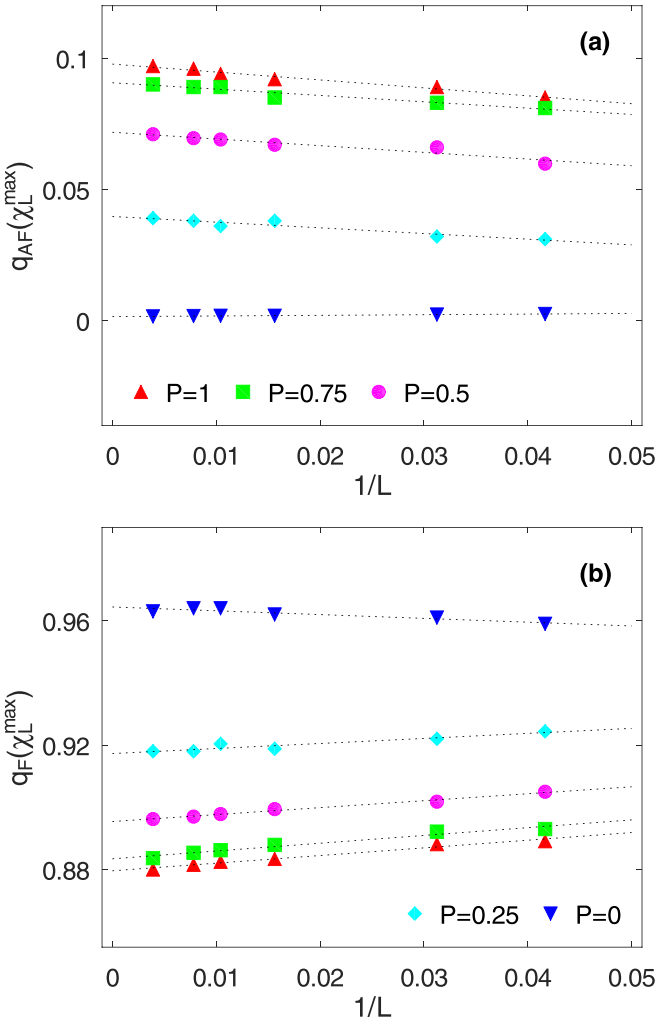

FIG. 4. Extrapolation of the critical transition probability q_c obtained for linear lattice sizes $24 \leqslant L \leqslant 256$ and for different values of p as indicated in the figures. (a) The points in the transition between AF-P phases are represented, and (b) the points in the transition between the P-F phases. The values of critical transition probabilities $q_c(L \to \infty)$ can be seen in Table I and Table II, respectively.

With the critical point values, we built the phase diagram which shows the regions on the plane of T versus q, where the F, P, and AF phases are found. The phase diagrams are presented in Fig. 5, for different values of p, where we can see the greater the probability of adding J_{ik}, the greater the region where we find the ordered phases.

TABLE II. Critical competition probability q_c, based on the extrapolating of the susceptibility discontinuity and in the F-P phase transition, for $T = 1$.

p	q_c^{χ}	β/ν	γ/ν	ν
0	0.964 ± 0.002	0.11 ± 0.02	1.67 ± 0.09	1.06 ± 0.09
0.25	0.917 ± 0.002	0.47 ± 0.06	1.01 ± 0.06	0.96 ± 0.09
0.5	0.895 ± 0.001	0.46 ± 0.02	1.04 ± 0.02	0.96 ± 0.09
0.75	0.883 ± 0.002	0.46 ± 0.01	1.06 ± 0.01	0.99 ± 0.06
1.0	0.880 ± 0.001	0.49 ± 0.01	1.0 ± 0.02	1.03 ± 0.04

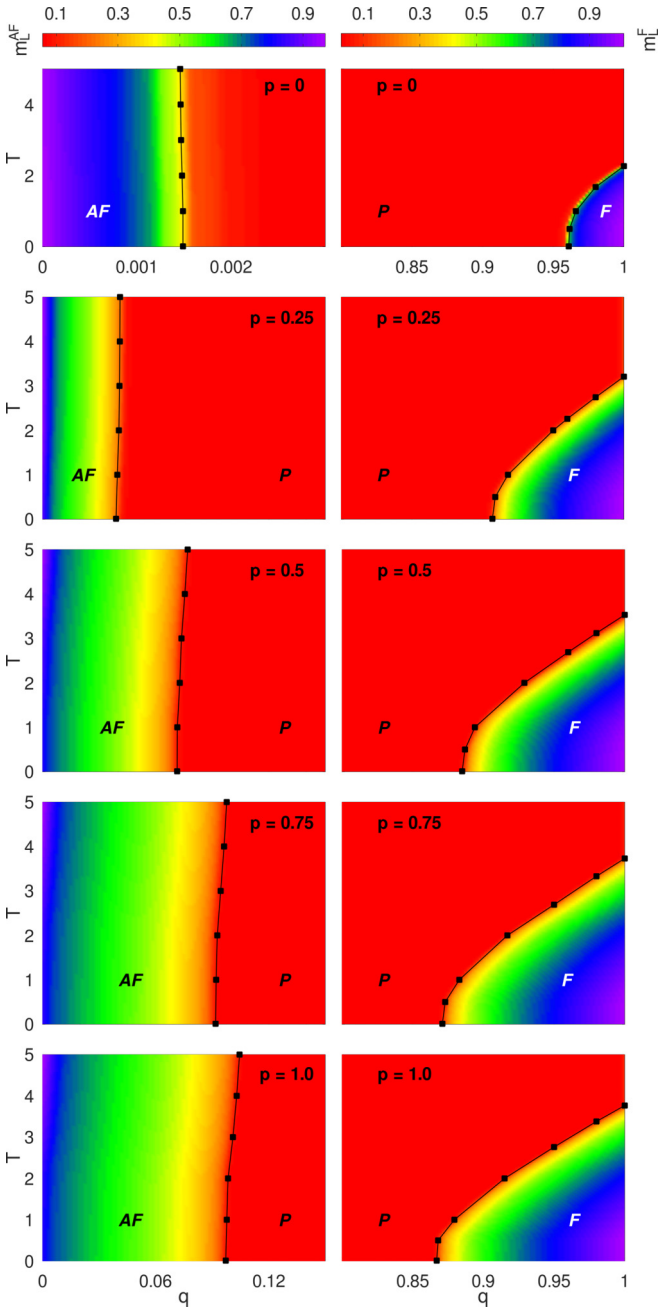

FIG. 5. Phase diagrams with different background colors for the phase transitions between the AF-P and P-F phases and for different values of p as indicated in the figures. The black lines are just a guide for the eye in the second-order phase transitions and the black square dots are critical points calculated. The color map refers to the magnetization of the system, m_L^{AF} and m_L^{F}, as indicated in the color bars.

Now, in order to better understand the behavior of these phases (see Fig. 5), we can relate these ordered phases to dynamics used in the competition. The AF phase, observing the q axis, is found when $q \to 0$ and the order parameter $m_L^{AF} \to 1$ (see the figures on the left side in Fig. 5), i.e., when the two-spin flip dynamic prevails in the competition. This

TABLE III. Critical competition probability q_c, based on the crossing of the fourth-order Binder cumulant curves and in the AF-P phase transition, for $T = 1$. The effective dimension is given by hyperscaling relation $d_{\text{eff}} = 2\beta/\nu + \gamma/\nu$.

p	q_c^U	β	$\nu(\text{m}^{\text{AF}})$	γ	$\nu(\chi^{\text{AF}})$	d_{eff}
0	0.00145 ± 0.00004	0.125 ± 0.03	1.0 ± 0.05	1.75 ± 0.04	1.0 ± 0.05	2.00 ± 0.21
0.25	0.0390 ± 0.0009	0.46 ± 0.06	0.96 ± 0.06	1.06 ± 0.05	1.0 ± 0.05	2.02 ± 0.29
0.5	0.0715 ± 0.0006	0.44 ± 0.05	1.0 ± 0.05	1.05 ± 0.03	1.0 ± 0.04	1.93 ± 0.24
0.75	0.0921 ± 0.0007	0.48 ± 0.04	0.98 ± 0.06	1.05 ± 0.06	1.0 ± 0.04	2.03 ± 0.31
1.0	0.0978 ± 0.0004	0.48 ± 0.03	1.02 ± 0.06	1.06 ± 0.06	0.98 ± 0.04	2.02 ± 0.23

is because, in the dynamic that simulates the system with an external energy flow into it, the change in the spin states is only accepted if it increases the energy of the system. Considering the Hamiltonian model, Eq. (1), the state of the highest energy to which the dynamics lead the system is the one where the spins are aligned antiparallel. The antiparallel order also can be achieved through the A-SWN, because if we analyze locally, the antiferromagnetic phase occurs when a central spin is in the up (down) state, and its neighbors, to whom it is connected, are in the down (up) state. Extending this analysis to the entire network, an ordering of this type only occurs when we have well defined what are the central spins and what sites they can connect to; otherwise, completely random long-range interactions can connect two distant sites in the network that the highest local energy configuration of one of these is unfavorable to the local antiparallel ordering of the other site, thus making it impossible to obtain the stationary state with an AF phase in the system. In this context, the F phase is found in the limit that $q \to 1$ and the order parameter $m_L^{\text{F}} \to 1$ (see the figures of the right side in Fig. 5), i.e., when the one-spin flip dynamic prevails. This dynamic is responsible for simulating the system in contact with the heat bath at temperature T and favors the lowest-energy state through the thermal equilibrium, in which all spins have the same state following the Hamiltonian system, so, if we wanted to, we could treat them without the sublattices in the A-SWN regime. On the other hand, when none of the dynamics prevails, i.e., between the extremes of the probability q value, not one of the expected order phase types is found in the system. Thus, we have most of the values of q, the P phase in the system is found, where both $m_L^{\text{AF}} \to 0$ and $m_L^{F} \to 0$. Another important observation is that the phase diagram topology changes when p increases, but the phases do not disappear.

After the presentation of the phase diagrams by exploiting the thermal variations of the order parameters, the Binder cumulant, and the magnetic susceptibility, we can now study the critical behavior of these quantities in the vicinity of the phase transitions using the FSS method to evaluate some critical exponents of the model. Therefore, to obtain the critical exponents, we also used two methods, both referring to the FSS method, using the scale relations of Eqs. (11), (12), and (14). One of the methods refers to the value of the thermodynamic quantities at the critical point, in which when we make a log-log plot of the value of these quantities as a function of L. Using the scale relations, we obtain ratios between the critical exponents through the slope of the line of best fit of those points. In Fig. 6, the behavior of thermodynamic quantities near the critical point can be seen as a function of L in the log-log plot. In Figs. 6(a) and 6(b) we were able to find the ratio $-\beta/\nu$ in the AF-P and F-P phase transitions, respectively, using the scaling relation of the Eq. (11), through the slope in the linear fit of the points for each selected value of p, as indicated in the figures. The same can be done using the scaling relation of Eq. (12); however, the critical exponent ratio is γ/ν and obtained by the slope of the linear fits of Figs. 6(c) and 6(d) for the different values of p and in the AF-P and F-P phase transitions, respectively. Finally, to the ratios between the exponents obtained previously, it is useful to use the scaling relation of Eq. (14), in which with the data of the Binder cumulant derivative we obtain information related to the critical exponent of correlation length, ν. Here they were obtained from the linear fit of the curves of Figs. 6(e) and 6(f) for the different p values and AF-P and F-P phase transitions, respectively. It is worth noting that as our interest is in the slope of the log-log plot, we changed the linear coefficients of the straight lines to separate the lines, thus making it easier for the reader to see the fits. All the ratios between the values of the critical exponents obtained by the log-log plot of the scaling relations can be seen in Table I for the AF-P phase transitions and in Table II for the F-P phase transitions.

Another method used to obtain the critical exponents is through the scaling functions in Eqs. (11), (12), and (14)

TABLE IV. Critical competition probability q_c, based on the crossing of the fourth-order Binder cumulant curves and in the F-P phase transition, for $T = 1$. The effective dimension is given by hyperscaling relation $d_{\text{eff}} = 2\beta/\nu + \gamma/\nu$.

p	q_c^U	β	$\nu(\text{m}^{\text{F}})$	γ	$\nu(\chi^{F})$	d_{eff}
0	0.965 ± 0.0004	0.125 ± 0.02	1.0 ± 0.05	1.70 ± 0.07	1.01 ± 0.03	1.95 ± 0.20
0.25	0.917 ± 0.0009	0.45 ± 0.05	1.0 ± 0.05	1.05 ± 0.05	1.0 ± 0.04	1.95 ± 0.26
0.5	0.895 ± 0.0008	0.46 ± 0.04	0.95 ± 0.07	1.05 ± 0.04	1.0 ± 0.04	2.02 ± 0.12
0.75	0.883 ± 0.0005	0.47 ± 0.03	1.0 ± 0.06	1.04 ± 0.06	1.0 ± 0.05	1.98 ± 0.23
1.0	0.879 ± 0.0006	0.49 ± 0.04	1.0 ± 0.07	1.02 ± 0.05	0.99 ± 0.06	2.00 ± 0.26

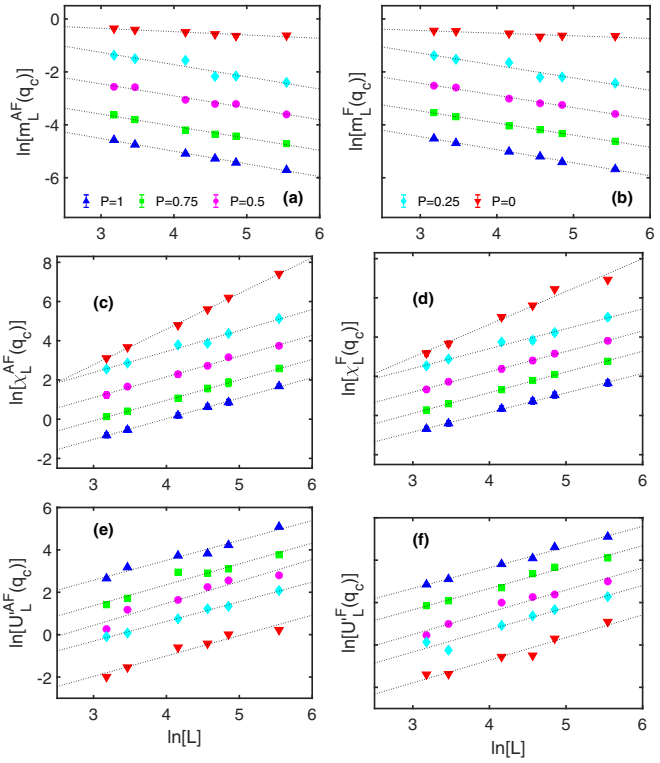

FIG. 6. (a) and (b) the best fit of the staggered m_L^{AF} and total m_L^{F} magnetization curves in the critical point as a function of the different values of L in the log-log plot, respectively, for the AF and F phases, in which the slopes we obtained the ratio β/ν between the critical exponents. (c) and (d) in the AF and F phases, we have the best fit of the staggered χ_L^{AF} L and total χ_L^{F} susceptibility curves at the critical point as a function of L, and the slopes have given us the ratio γ/ν. The critical exponent ν, we have obtained by the slope of the best fit of the Binder cumulant derivative U_L^{AF} and U_L^{F} at the critical point, as represented in (e) and (f) for the AF and F phases, respectively. The critical exponents obtained by this method for the AF phase can be seen in Table I and in Table II for the F phase.

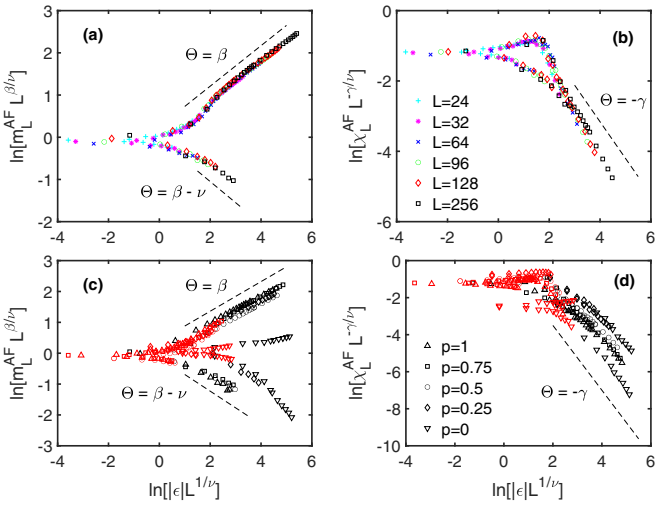

FIG. 7. Data collapse by FSS analysis for (a) staggered magnetization m_L^{AF} and (b) susceptibility χ_L^{AF} for different values of L as indicated in the figure and fixed $p = 0.75$. (c) and (d) the data collapse for m_L^{AF} and χ_L^{AF}, respectively, but for all values of p, in which the critical exponents were obtained using the best data collapse for all lattice sizes, and here we only display the lattice sizes $L = 24$ [red (light gray) symbols] and $L = 256$ (black symbols). The ε parameter is set to $\varepsilon = (q - q_c)/q_c$. The dashed lines represent the asymptotic behavior of the scale functions. The values of the critical exponents β, γ, $\nu(\mathrm{m}_L^{\mathrm{AF}})$, and $\nu(\chi_L^{\mathrm{AF}})$ of the best data collapse can be seen in Table III.

around the critical point. For this, we isolate the scale function and plot it in a log-log plot through the curves of $m_L L^{\beta/\nu}$ and $\chi_L L^{-\gamma/\nu}$ as a function of $|\varepsilon|L^{1/\nu}$, resulting in a single curve for all lattice sizes L if we have the correct critical exponents and critical points adjusted in the scaling relations. In this method, the data collapse can also be obtained in a plot that does not have the axes on the logarithmic scale, but the asymptotic behavior that relates to the critical exponents are not present. We can obtain the critical exponents because the data collapse in the vicinity of the critical point depends on the correct critical exponents of the system to occur, and, in this way, we adjust them to obtain the best data collapse in the criticality. Consequently, the exponents involved in this data collapse are the critical exponents of the system. All values of the critical exponents obtained by data collapse of the scaling relations can be seen in Table III for the AF-P phase transitions (β, $\nu(m^{\mathrm{AF}})$, $\nu(\chi^{\mathrm{AF}})$, γ) and in Table IV for the F-P phase transitions (β, $\nu(m^{\mathrm{F}})$, $\nu(\chi^{\mathrm{F}})$, γ).

In Fig. 7, we have shown the data collapse for the scaling functions of magnetization, Fig. 7(a), and for magnetic susceptibility, Fig. 7(b), for the AF-P phase transition, with $p = 0.75$, which was the best data collapse obtained. In this phase transition, we also plotted for all values of $0 \leqslant p \leqslant 1.0$, as can be seen in Fig. 7(c) and 7(d), the scaling function of magnetization and magnetic susceptibility, respectively, showing the best data collapse for the selected p values but displaying only the lattice sizes $L = 24$ [red (light gray) symbols] and $L = 256$ (black symbols) for the best differentiation between the collapsed curves.

However, in the F-P phase transition, the figures that present the best data collapse, for $p = 0.75$, are Fig. 8(a) for the magnetization scaling function, and Fig. 8(b) for the magnetic susceptibility scaling function. We also have calculated for all values of $0 \leqslant p \leqslant 1.0$, but also only displaying here two lattice sizes, $L = 24$ [red (light gray) symbols] and $L = 256$ (black symbols), and they can be found in Figs. 8(c) and 8(d) for the magnetization and the magnetic susceptibility scaling functions, respectively. The critical exponents obtained by this method, data collapse, can be found in Table III for AF-P phase transitions and in Table IV for phase transitions from F to P.

In both methods, we obtained very approximate values for the critical exponents for the selected p values. The best results shown here are based on data collapse; this is due to the fact that for $p = 0$ the values of the critical exponents are closer to the values of the Ising model on the regular square lattice, which they are known by exact solution and MC simulation, $\beta = 1/8$, $\gamma = 7/4$, and $\nu = 1$. On the other hand, when we increase the additive probability p, we also increase the number of J_{ik} added to the system, and, thus, it is convenient to use the scaling relations of systems that can have mean-field

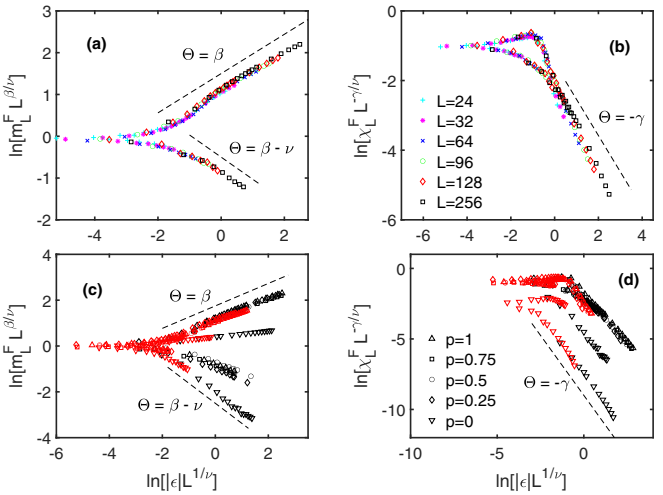

FIG. 8. Data collapse by FSS analysis for (a) total magnetization m_L^F and (b) susceptibility χ_L^F for different values of L as indicated in the figure and fixed $p = 0.75$. (c) and (d) the data collapse for m_L^F and χ_L^F, respectively, but for all values of p, in which the critical exponents were obtained using the best data collapse for all lattice sizes, and here we only display the lattice sizes $L = 24$ [red (light gray) symbols] and $L = 256$ (black symbols). The ε parameter is set to $\varepsilon = (q - q_c)/q_c$. The dashed lines represent the asymptotic behavior of the scale functions. The values of the critical exponents β, γ, $\nu(m^F)$, and $\nu(\chi^F)$ of the best data collapse can be seen in Table IV.

critical behavior by the prediction that we have a system above the Ising model upper critical dimension, $d = 4$, in the A-SWN regime. To do that, it is enough in the scaling relations, Eqs. (11), (12), and (14), to substitute the linear length L of the lattice by the total number of spins in the system, $L^2 = N$. By doing this, as predicted, are obtained approximately the mean-field critical exponents $\beta = 1/2$, $\gamma = 1$, and $\nu = 1/2$. The behavior of both the critical exponents for $p = 0$ and the A-SWN regime ($0 < p \leqslant 1$) were represented in Fig. 9(a) for the AF-P phase transition and in Fig. 9(b) for the F-P phase transition.

The critical exponents are not independent of one another but related by simple scaling laws, as is the case with the hyperscaling law $d_{\text{eff}} = 2\beta/\nu + \gamma/\nu$, in which we have as a result the effective dimension d_{eff} of the system. With this law, we see that the system has approximately the same critical exponents in the A-SWN regime, as we are returned that $d_{\text{eff}} \cong 4.0$ with the mean-field critical exponents, and $d_{\text{eff}} \cong 2.0$ for $p = 0$, following the data in the Tables III and IV, obtained with the scale relations of Eqs. (11), (12), and (14).

The universality class can be defined by the set of exponents in the phase transition, as in the case of the second-order phase transitions, in which systems that are very different from each other can share the same set of critical exponents. In general, these systems share the same spatial dimension, symmetries, and ranges of interactions. Here, following the set of critical exponents obtained at $p = 0$, we have the same universality class of the equilibrium Ising model in the regular square lattice. However, in the A-SWN regime ($0 < p \leqslant 1$), we have long-range interactions in the system, and, due to its consequent set of critical exponents, the system belongs to the

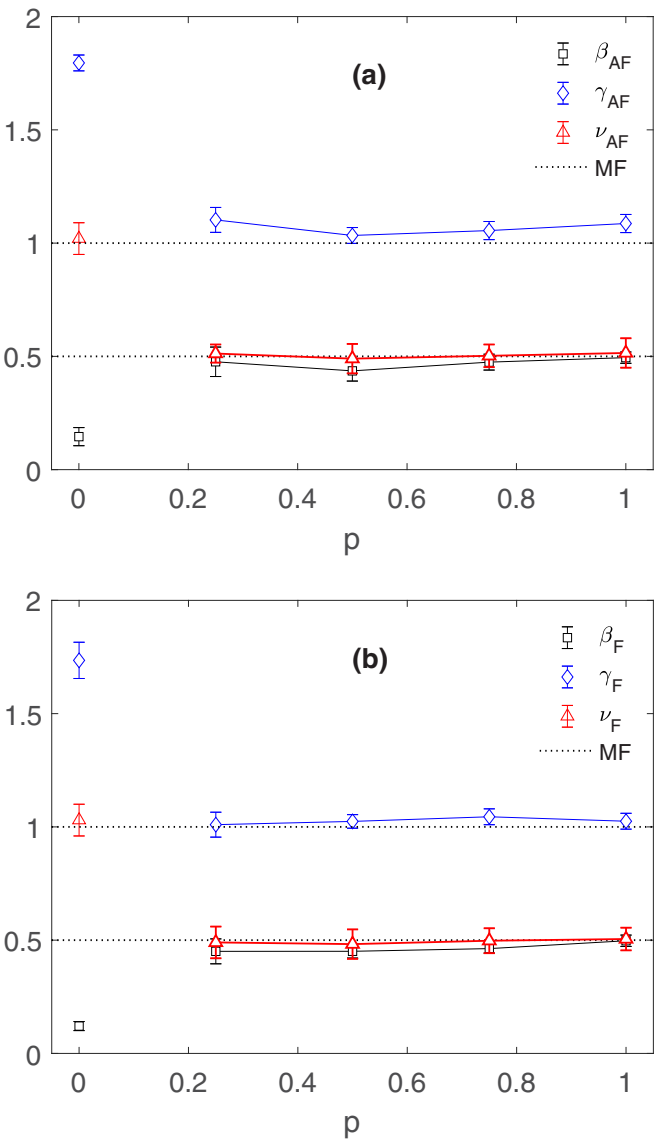

FIG. 9. (a) Representation of the critical exponents presented in Tables III and I for the critical behavior of the system in the AF-P phase transition, taking into account the mean-field scale relationships for the A-SWN regime ($0 < p \leqslant 1$). (b) Representation of the critical exponents presented in Tables IV and II for the system in the F-P phase transition, also using the mean-field scale relations in the A-SWN regime ($0 < p \leqslant 1$). In both figures, we have the comparison with the mean-field critical exponents (MF) by the dotted lines, $\gamma = 1.0$ and $\beta = \nu = 0.5$.

mean-field universality class. By comparing with the results obtained for the Ising model in the two-dimensional A-SWN at the thermodynamic equilibrium regime [24,28], we see that both the nonequilibrium model and the equilibrium model have the same universality class, the mean-field universality class, in stationary critical behavior.

V. CONCLUSIONS

In this work, we have developed MC simulations to study the thermodynamic quantities and the critical behavior of the nonequilibrium Ising model on a 2D A-SWN. By using the

one- and two-spin flip competing dynamics we reach the stationary state of the system at the nonequilibrium regime. We have found two types of phase transitions, from P to AF and from P to F phases, when the two-spin flip dynamic prevails in the system and when the one-spin flip prevails in the system, respectively. To find the phases we have used the total and staggered magnetizations per spin, and its respective susceptibility and reduced fourth-order Binder cumulant, both as a function of the competition parameter q. With the last two quantities we obtained the critical points of the system and we built the phase diagrams of the system. We have observed that increasing the coordination number of the network by adding long-range interactions to our A-SWN, with addition probability p, we also increase the regions of the ordered phases on the diagram.

Here we could have used the Kawasaki mechanism instead the two-spin flip mechanism, because we only have one type of spin in the lattice. If we had used the Kawasaki mechanism, then the phases diagram undergoes a modification, and now, that dynamic prevailing in the competition, the magnetization and, consequently, the ordered phases of the system will depend on its temperature. This dependence with the temperature is due to the one-spin flip mechanism, which favors the lowest-energy state, and in lower temperatures all spins are parallel, i.e., always have the F phase, and only have the possibility of the AF phase in high temperatures [26].

Through the FSS arguments, we calculated the critical exponents β, γ, and ν of the system, and for the A-SWN regime ($0 < p \leqslant 1$) we obtained the same exponents of a system with mean-field critical behavior, except for $p = 0$, where, as expected, we obtained the critical exponents of the Ising model in a regular square lattice. Thus, in the A-SWN regime, we have concluded that the nonequilibrium system is in the mean-field universality class, as the equilibrium system in the A-SWN [24,28]. That equivalence between the critical behavior of the equilibrium and nonequilibrium models was already predicted and observed in other systems [4–8]. It is also important to specify that our results concerning the regions of the phase diagram based on the changes in the critical points, and the mean-field behavior, is in agreement with the observed behavior of disorder with shortcuts added to the Ising model in a SWN [12,18,20–22,24,28].

The change in the critical behavior is directly related to the network structure of the system, more specifically, in the study of the free scale networks, it is shown that the criticality of systems is very dependent on the degree distribution of the network [29]. If the fourth moment of the degree distribution in the network is convergent, then a critical mean-field behavior is observed in the system; otherwise, the existence and kind of criticality is decided by the number of the more connected sites in the network. For that, due the fact that our network has a bimodal distribution, its fourth moment is convergent and explains the critical mean-field behavior obtained in our work.

ACKNOWLEDGMENTS

This work has been supported by the following Brazilian research agencies: FAPEMAT, CAPES-Finance Code 001, and CNPq.

[1] R. J. Glauber, J. Math. Phys. **4**, 294 (1963).
[2] K. Kawasaki, Phys. Rev. **145**, 224 (1966).
[3] W. Figueiredo and B. C. S. Grandi, Braz. J. Phys. **30**, 58 (2000).
[4] G. Ódor, Rev. Mod. Phys. **76**, 663 (2004).
[5] T. Tomé and M. J. de Oliveira, Phys. Rev. A **40**, 6643 (1989).
[6] B. C. S. Grandi and W. Figueiredo, Phys. Rev. E **53**, 5484 (1996).
[7] M. Godoy and W. Figueiredo, Phys. Rev. E **66**, 036131 (2002).
[8] M. Godoy and W. Figueiredo, Phys. Rev. E **65**, 026111 (2002).
[9] S. Mingram, Psychol. Today **1**, 61 (1967).
[10] D. J. Watts and S. H. Strogatz, Nature (Lond.) **393**, 440 (1998).
[11] M. E. J. Newman and D. J. Watts, Phys. Rev. E **60**, 7332 (1999).
[12] S. N. Dorogovtsev, A. V. Goltsev, and J. F. F. Mendes, Rev. Mod. Phys. **80**, 1275 (2008).
[13] A. D. Sánchez, J. M. López, and M. A. Rodríguez, Phys. Rev. Lett. **88**, 048701 (2002).
[14] M. Dupont and N. Laflorencie, Phys. Rev. B **103**, 174415 (2021).
[15] B. J. Zubillaga, A. L. M. Vilela, M. Wang, R. Du, G. Dong, and H. E. Stanley, Sci. Rep. **12**, 282 (2021).
[16] E. M. S. Luz and F. W. S. Lima, Int. J. Mod. Phys. C **18**, 1251 (2007).
[17] A. Pękalski, Phys. Rev. E **64**, 057104 (2001).
[18] H. Hong, B. J. Kim, and M. Y. Choi, Phys. Rev. E **66**, 018101 (2002).
[19] F. W. S. L, Res Med Eng Sci. **3**, RMES.000553 (2017).
[20] A. Barrat and M. Weigt, Eur. Phys. J. B **13**, 547 (2000).
[21] C. P. Herrero, Phys. Rev. E **65**, 066110 (2002).
[22] M. Gitterman, J. Phys. A: Math. Gen. **33**, 8373 (2000).
[23] J. Viana Lopes, Y. G. Pogorelov, J. M. B. Lopes dos Santos, and R. Toral, Phys. Rev. E **70**, 026112 (2004).
[24] X. Zhang and M. Novotny, Braz. J. Phys. **36**, 664 (2006).
[25] W. Liu, W.-Y. Xiong, and J.-Y. Zhu, Phys. Rev. E **71**, 056123 (2005).
[26] W. Liu, Z. Yan, and G. Zhou, Open Phys. **17**, 1 (2019).
[27] J.-Y. Zhu, W. Liu, and H. Zhu, Eur. Phys. J. B **36**, 545 (2003).
[28] R. A. Dumer and M. Godoy, Eur. Phys. J. B **95**, 159 (2022).
[29] A. V. Goltsev and S. N. Dorogovtsev, and J. F. F. Mendes, Phys. Rev. E **67**, 026123 (2003).
[30] K. Binder and D. W. Heermann, *Monte Carlo Simulation in Statistical Physics*, *An Introduction*, 6th ed. (Springer, Cham, Switzerland, 2019).
[31] K. Binder and D. P. Landau, *A Guide to Monte Carlo Simulations in Statistical Physics*, 4th ed. (TJ International Ltd, Padstow, UK, 2015).
[32] L. Böttcher and H. J. Herrmann, *Computational Statistical Physics*, 1st ed. (Cambridge University Press, New York, 2021).
[33] S.-H. Tsai and S. R. Salinas, Braz. J. Phys. **28**, 58 (1998).